# Metamorphic dehydration reactions trigger slow slip events in subduction zones

Jorge Jara[1], Mathieu Soret[1], Romain Jolivet[1], Nadaya Cubas[1], Andrei Maksymowicz[1], and Fabrice Cotton[1]

[1]Affiliation not available

November 17, 2025

# Metamorphic dehydration reactions trigger slow slip events in subduction zones

J. Jara[1*], M. Soret[2], R. Jolivet[2,3], N. Cubas[4], A. Maksymowicz[5], F. Cotton[1,6]

[1] GFZ Helmholtz Centre for Geosciences, Telegrafenberg, 14473, Potsdam, Germany.

[2] Laboratoire de Géologie, Département de Géosciences, École Normale Supérieure, PSL Université, Paris, France.

[3] Institut Universitaire de France, Paris, France.

[4] CNRS-INSU, Institut des Sciences de la Terre Paris, Sorbonne Université, ISTeP UMR 7193, Paris, France.

[5] Departamento de Geofísica, Facultad de Ciencias Físicas y Matemáticas, Universidad de Chile,

Blanco Encalada 2002, Santiago 8370449, Chile

[6] Institute of Geosciences, University of Potsdam, Potsdam, Germany.

*Corresponding author. Email: jorge@gfz.de

**Slow Slip Events (SSEs), widespread along most subduction zones, play a critical role in the seismic cycle as they are known to gradually release stress and trigger earthquakes. Yet, the conditions driving SSEs remain poorly constrained. Here, based on thermal state modeling of subduction zones worldwide, we reveal that SSEs predominantly occur within two clusters at ~100°C and ~450±100°C. Using phase equilibrium modeling, we show that these clusters distribute where significant dehydration reactions are expected in subducting metasedimentary and oceanic crustal rocks. These findings are consistent with geological observations from exhumed subduction interfaces, laboratory experiments and numerical modeling indicating that mineral transformations and associated fluid release can promote SSE nucleation by locally and transiently weakening the megathrust.**

Since its early discovery along continental faults (*1*), aseismic slip has been recognized globally as a key element of the earthquake cycle, significantly challenging the vision of the Elastic Rebound proposed by Reid in the aftermath of the 1906 San Francisco earthquake (*2*). Aseismic slip accommodates part of the elastic energy that accumulates during the interseismic period (*3, 4*), in the form of steady-state creep, Slow Slip Events (SSEs) or afterslip. Aseismic slip is also a key component to consider in seismic hazard, as it has been proposed as a mechanism that can, in some cases, trigger earthquakes (*5, 6*), as well as impact probabilistic hazard assessment (*7*). SSEs correspond to a transient acceleration of slip along a portion of an active fault over a finite period during which slip remains at subseismic speeds, hence without radiating seismic waves. Although detected along all types of faults globally (*8*), SSEs have been primarily observed and modeled in subduction zones, where dense geodetic networks enable their detection and characterization (*4, 8, 9*).

Despite such scrutiny, the physical processes that control SSEs remain poorly understood and are still debated across disciplines, including geophysics, earthquake mechanics, and field-based geology. For instance, it remains unclear whether SSEs correspond to a slip instability on a frictional interface (*10, 11*) or a shear instability affecting a wider deformation zone (*12, 13*). Furthermore, we do not know whether shallow (less than 15 km depth) and deep (more than 40 km) SSEs are equivalent in that regard. In any case, some ingredients are necessary for a model to explain the nucleation and propagation of SSEs from a geodetic perspective. First, the megathrust must be able to build up stress under tectonic motion and a transient weakening mechanism is required to explain the release of the corresponding available elastic energy. Second, if SSEs are frictional slip instabilities, a mechanism, potentially different, is needed to maintain slip at subseismic speeds. Finally, the material in which SSEs originate and grow may be relatively weak as the stress drop of SSEs is generally not larger than a few kPa (*14*), orders of magnitude smaller than those of classic earthquakes.

Following this, three main families of models have been proposed to explain the occurrence of SSEs. The first group of models involves the presence of fluids within fault zones (*4, 13*). Elevated pore fluid pressure effectively weakens brittle faults by decreasing the effective normal stress, promoting slip (*11, 15, 16*) as well as increasing the nucleation length, the size over which a slip instability should grow to become dynamic and start to radiate seismic waves (*17, 18*). Dilatant strengthening has also been proposed as a means to quench the slip instability by self-modulation of

the pore pressure by the propagating rupture itself (*19*). Fluids are also known to reduce the strength of viscous shear zones, which could explain the occurrence of shear instabilities (*20, 21*). The second group of models relates to stress interactions arising from fault geometric complexities (*22, 23*). Faults and shear zones are not simple planar structures; instead, fractures and damage zones interact with the fault core, facilitating the localization of deformation that triggers SSEs (*24*). The third group of models includes heterogeneities in the constitutive properties of fault materials, which may lead to localized slip instabilities on short timescales (*25, 26*). All of these models may explain geodetic observations of SSEs and be consistent with the seismological signature of slow slip. However, many of the proposed physical conditions rely on field-based observations of exhumed fossil plate interfaces and the role of fluids, in particular, remains difficult to quantify. Although rock dehydration is commonly cited as the primary fluid source at the subduction interface (*27, 28*), evidence linking these fluids to SSEs is still scarce (*13, 29*).

Decades of thermal modeling and field observations have constrained the pressure–temperature (P–T) conditions of subduction interfaces, identifying depths where dehydration reactions are expected. Building on this framework, we combine thermal modeling with a global compilation of SSEs to evaluate their relationship with metamorphic processes. Our results show that SSEs preferentially occur within two P–T ranges corresponding to zones of preferential dehydration of subducting clays and oceanic crust.

## Thermal modeling of subduction zones

We implement a thermal model for nine subduction zones around the Pacific region where SSEs have been reported (*30, 31*) (Japan Trench, Nankai, Ryukyu, New Zealand, Alaska, Cascadia, Mexico, Costa Rica and Peru-Chile; Fig.1). The geometry of the plate interface is defined using Slab2.0 (*32*), which we mesh into triangular elements of variable size (approximately 5 $km^2$ near the coast and up to 30 $km^2$ near the trench and at greater depths; figs. S1 to S8). This discretization provides a set of points along the slab interface at which we estimate the temperature using analytical expressions that solve the steady-state heat advection–diffusion equation, incorporating the effects of shear heating and slab curvature (*33–35*) (Supplementary Materials).

Our thermal modeling incorporates spatially variable inputs at each node along the subduction

interface, including plate age, convergence velocity, distance from the trench, density, and shear stress. It also accounts for the average thermal conductivity of both the upper plate and the top of the subducting plate, as well as thermal diffusivity. To assess uncertainties in the final temperature estimates, each input parameter is considered as normally distributed around its mean value (Supplementary Materials). We sample the corresponding distribution of input parameter and derive, for each sample, the corresponding thermal conditions at depth. This approach yields the spread of possible thermal models for each of the subduction zones considered in this study (Fig.1; figs. S9 to S16). Our predictions and associated uncertainties are consistent with previously published models in these regions (*11, 33–37*).

## SSE observations and thermal models

We compile approximately 2700 SSEs from a global database within the nine subduction zones targeted in this study (*30,31*) (Supplementary Materials). To account for uncertainties in location, we generate 50,000 samples by treating each SSE location as a bivariate normal distribution centered on the reported epicenter, with a spatial covariance of 10 $km^2$. This approach helps mitigate potential biases in assigning SSE depths. Each sample is then projected onto the slab interface defined for its respective subduction zone, where its location along the interface is used to interpolate temperature from the thermal model. By focusing on the epicentral location, we explicitly target the nucleation point of each SSE, rather than its entire spatial extent or propagation history. This procedure yields a temperature, along with its associated uncertainty, for each SSE (Fig.1; figs. S9 to S16).

The resulting P-T paths for the nine studied subduction zones are shown in the central panel of Fig. 1. We then evaluate the probability density function (PDF) of the temperature associated with all SSEs within each subduction zone. To characterize these distributions, we apply a Gaussian Mixture Model to identify the number and mean values of underlying normal components. Six subduction zones (Cascadia, Mexico, Costa Rica, Nankai, New Zealand, and Peru–Chile) show bimodal temperature distributions, with Gaussian means centered between 100–420°C and 300–520°C. In contrast, Alaska, the Japan Trench, and Ryukyu display trimodal distributions, with Gaussian means around 60–100°C, 200–530°C, and 370–980°C. Despite this variability, no systematic thermal pattern emerges from the regional comparisons, suggesting that temperature alone

does not uniquely constrain the occurrence of SSEs across subduction zones.

Building on these observations, we estimate the P–T distribution of all SSEs under the assumption of lithostatic pressure, which provides a broader view of the conditions under which SSEs occur, although no single dominant pattern is apparent (Fig. 2A). We compute the marginal PDFs of pressure and temperature independently. While the pressure PDF does not display any distinct features (Fig.2B), the PDF of temperature reveals two distinct peaks, centered at approximately 100°C and 460°C (Fig. 2B). To jointly assess the influence of pressure and temperature, we construct the PDF of SSEs occurrence in the P-T space using a kernel density estimate (KDE; Fig.2B). The PDF exhibits two principal modes, including a well-defined one centered near 100°C and 0.3 GPa, and a second one, more diffuse, spanning temperatures between 350°C and 550°C and pressures between 0.9 and 1.3 GPa (Fig.2B). In order to further characterize the physical conditions of the habitat of SSEs, we perform petrological modeling to quantify the amount of fluids released by a subducting oceanic crust crossing the P–T fields associated with these regions identified as preferentially hosting SSEs.

## SSEs and Thermodynamic Modeling

We use the Perple_X software (*38*) to perform phase equilibrium modeling and compare the stability conditions of major mineral phases predicted at the top of the subducting plate with our compilation of SSEs. Using an internally consistent thermodynamic dataset (hp62ver.dat) (*39*), we calculate pseudosections (Fig.2B, and fig. S17) for two representative compositions of subducted metasediments of oceanic affinity (*40*) and mid-ocean ridge basalts (MORB) (*41*), in the MnNCKFMASHT and NCKFMASHT systems, respectively. In particular, we focus on the evolution of structurally bound $H_2O$ content (in wt.%) as a function of P, T and dehydration reactions for sub-solidus conditions (200–650°C and 0.1–3 GPa). Fig. 3A and Fig. 3B illustrate this evolution along a linear thermal gradient of 13°C/km for both lithologies, from 200°C–0.4 GPa to 650°C–1.5 GPa.

Results from phase equilibrium modeling reveal that the deep cluster of SSEs (350-550°C) coincides with major dehydration reactions under greenschist-facies conditions. SSEs are comparatively scarce at blueschist-facies conditions (≤350–400°C) where mafic rocks and sediments

are highly hydrated but dehydration reactions are limited. For both lithologies, metasediments and basalts, the onset of dehydration occurs near the downdip limit of the seismogenic zone (T ~350°C) with the breakdown of two key hydrous phases: pumpellyite and lawsonite, which contain ~6 and ~12 wt.% structurally bound $H_2O$, respectively. Subsequent dehydration at higher temperatures (and pressures) is primarily driven by the breakdown of chlorite, which also contains ~12 wt.% structurally bound $H_2O$. In mafic rocks, chlorite breakdown releases substantial fluid at two distinct temperatures (T ~410 and ~500°C), whereas in sediments, chlorite destabilization proceeds more gradually and at slightly higher metamorphic grades (T ~475–590°C; fig. S17). SSEs become increasingly rare at amphibolite-facies (or eclogite-facies) conditions (≥ 500–550°C) where both mafic rocks and sediments are largely dehydrated. Indeed, dehydration reactions at greenschist-facies conditions account for the majority of fluid release (~60–70% of the initial $H_2O$ content) from both lithologies along deep subduction interfaces (T ≥ 200°C).

Similar to the deep cluster of SSEs, the shallow one (centered around 100°C) correlates with conditions of elevated fluid release driven by sediment compaction and/or major dehydration reactions in clay-rich lithologies such as the smectite-to-illite transformation (*16, 42–44*) (Fig.3A).

## Discussion

### Metamorphic dehydration as a trigger for SSEs

The nine subduction zones analyzed in this study consistently show a strong spatial and thermal alignment between the location of SSEs and major dehydration reactions predicted from thermodynamic modeling. This observation corroborates previous studies based on different thermal models for warm subduction zones (*28*). Mafic rocks and sediments at the top of the downgoing plate preferentially react and dehydrate in both shallow and deep SSE regions (Fig.3A and B). Considering that our investigation focuses on the earliest stages (i.e., nucleation region) of SSEs, the observed alignment may be explained by two distinct, yet not mutually exclusive, mechanisms.

Where fluid is released along the megathrust, pore pressure increases and effective normal stress on the fault is reduced, thereby promoting a slip instability at a slow pace. Such mechanism would explain the occurrence of SSEs as frictional slip in a high pore fluid pressure environment (*28, 29, 45, 46*). Transient deformation may also be driven by the mineral transformation itself.

Field-based studies on fossil subduction zones as well as high-pressure deformation experiments reproducing natural shear zones indicate that fluid-assisted dissolution and precipitation (or pressure solution) processes can promote transient strain localization by weakening the stressed rocks in a semi-viscous regime (*21, 47*). Whether fluids or metamorphic reactions themselves provide the dominant weakening, dehydration is the primary cause of instability initiation once pore pressure reaches a critical level.

While we have considered the onset of slow slip, we now must discuss its subsequent slow propagation. The local conditions in the two identified P-T regions may favor distinct mechanisms that keep slip slow after its initiation. It turns out that the fluid-rich environment resulting from dehydration reactions acts in favor of maintaining slip to a low, subseismic speed. Considering frictional slip, a large nucleation length inhibits the transition to a dynamic rupture (*17, 48*), resulting in slow stress release along the fault. Such large nucleation size may result directly from material properties or, once again, from an elevated pore fluid pressure. One may also invoke the balance between dilatant strengthening and the prevailing P–T conditions to regulate slip rate locally. As deformation localizes, dilatancy increases, raising normal stress and counteracting further acceleration (*19, 49*). In the presence of fluids, the local increase in stress at the tip of the rupture may lead to a pore pressure increase, which would in turn again lengthen the nucleation size.

Together, these insights suggest that while metamorphic reactions can trigger SSEs, their persistence as slow events is governed by fault zone properties, including its constitutive properties, its fluid content and its geometry.

**Are all SSEs frictional?**

In all subduction zones worldwide, rocks become eventually viscous as temperature increases with depths and, in all subduction zones worldwide, rocks transition in the P-T diagram and undergo metamorphic reactions. The fact that we do not observe significant SSEs in all subduction zones worldwide is therefore puzzling. Metamorphism being considered as ubiquitous, we should observe SSEs everywhere if metamorphic reactions were to trigger SSEs. To understand this apparent dilemma, we must consider the nature of the deformation along the megathrust during a SSE. Shallow SSEs occur in the brittle regime, hence they must be frictional (*11, 12, 27, 46*), although

some studies suggest that viscous processes such as pressure-solution creep may also contribute at shallow depth or in mixed brittle–ductile environments (*50, 51*). For the deeper ones, the answer is twofold.

First, we may consider that deep SSEs are frictional events along a given interface. Based on thermo-petrological modeling of the subduction megathrust, it has been inferred that SSEs occur where the megathrust is made frictional at depth because of the presence of elevated pore fluid pressure (*11*). In this model, the transient nature of SSEs is explained by the spontaneous weakening of the megathrust interface, the latter being frictional at great depths because of a local elevated pore pressure. Slip remains slow because of material properties, in particular because of the mantle wedge corner serpentinites (*11*). In cold subduction zones, where dehydration reactions are limited at blueschist-facies conditions, such a frictional region may not develop; consequently, classical earthquakes rather than SSEs are observed, as along the Japan Trench (*11*). It is important to note that the sole presence of a frictional domain does not explain why slip events stay slow. In addition to this model (*11*), our observations suggest that the slow nature of SSEs primarily derives from elevated pore fluid pressure, generated by dehydration reactions, which increases the nucleation size along a frictional interface. The transient nature of the deformation could arise from the continuous release of fluids by metamorphic reactions, which would progressively approach the megathrust to failure. Through dilatancy, slip may modulate pore pressure and/or fluids could escape during the slip episode, before continuous fluid release leads to another pore pressure build up. Such mechanism could explain the apparent periodicity of SSEs in some places.

Second, we may consider that deep SSEs are the transient deformation of a broad shear zone. Weakening in the viscous regime can induce fast and transient deformation within a given volume (*21*), which, through strengthening induced by locally and transiently higher straining rates, may eventually end up triggering a slip instability akin to SSEs. SSEs may hence be seen as shear deformation across a broad shear zone, potentially involving semi-brittle or viscous mechanisms (*12, 13, 29, 50, 52, 53*). In such case, one must explain the transient nature of deformation one way or another. If we consider that the metamorphic reactions themselves locally weaken the fault material, then understanding the kinetics of metamorphic reactions becomes crucial to explain the transient behavior. One may consider a mineralogical assemblage that would remain metastable for some time while going down in subduction and suddenly react and release fluids to explain the transient nature

of SSEs. Such considerations may be supported by the apparent transient nature of aseismic slip as pointed out by the observed coalescence of small slow events to form larger SSEs in Mexico (*8*). In such a framework, deep aseismic slip would correspond to constantly reacting materials in a continuously sheared zone while SSEs would correspond to transiently reacting materials and/or lithologies that are prone to releasing large amounts of fluids at specific depths/thermal conditions.

As a conclusion on this point, the global distribution of SSEs supports the view that metamorphic dehydration plays a first-order role in their occurrence (Fig.3), but it does not uniquely constrain their mechanical nature. We note, however, that our thermodynamic modeling considers only two representative slab-top compositions (MORB and pelite). Carbonate- and quartz-rich lithologies (e.g., marble, quartzite) are nominally anhydrous and will not undergo the same dehydration reactions; if such rocks dominate the slab top, different physical and chemical behaviors are expected, which may help explain the lack of SSEs in some subduction zones, in addition to the rheology of the interface (*11*). That said, shallow SSEs (Fig.3A) are most consistently explained as frictional instabilities in clay-rich, overpressured sediments, whereas deeper events may correspond either to frictional slip patches sustained by high pore fluid pressure or to transient deformation within broad semi-brittle to viscous shear zones (Fig.3B). In both cases, the coincidence of SSEs with major dehydration reactions highlights that fluids—and their impact on pore fluid pressure—are the primary ingredient enabling slow slip, while the precise deformation mode likely depends on local lithology, fault-zone heterogeneity, and thermal conditions.

## Conclusions

Our results identify a consistent spatial and thermal alignment between SSE nucleation and pressure–temperature conditions favorable for metamorphic dehydration reactions in subduction zones. By systematically integrating thermal models with a global SSE database, we demonstrate that most events initiate within P–T domains characterized by elevated water release from dehydration processes in both metasediments and mafic rocks. In particular, we identify the smectite-to-illite transformation and the breakdown of pumpellyite, chlorite and lawsonite as good candidates for the shallow ($\sim$100°C) and deep clusters of SSEs (450$\pm$100°C), respectively. This suggests that major dehydration reactions, either through localized pore fluid pressure or physicochemical weakening during mineral transformations, contribute to triggering slip instabilities along narrow regions of

the megathrust. Whether such instabilities are purely frictional or involve mixed frictional–viscous behavior likely depends on depth, lithology, and fault-zone heterogeneity. This work underscores the value of interdisciplinary approaches that combine geophysical observations, thermal modeling, and petrological insights. By bridging these domains, we identify key conditions that provide critical constraints for mechanical models of SSEs and for earthquake hazard assessment. Such integration is essential for building a more comprehensive understanding of slow deformation phenomena along subduction zones and their associated hazards.

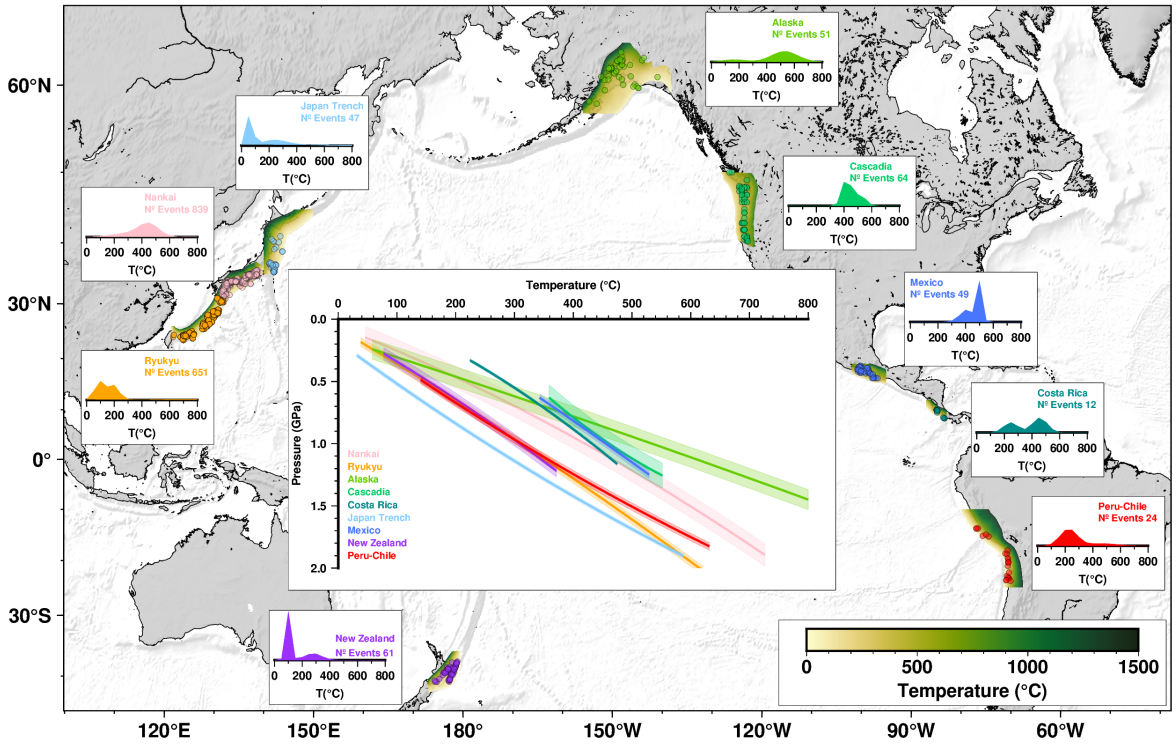


**Figure 1**: **Distribution of Slow Slip Events (SSEs) and associated temperature conditions across major subduction zones.** SSE locations are depicted along nine subduction zones, with color-coding representing the estimated temperature at the slip interface (indicated by dots). Insets illustrate the probability density function (PDF) of temperature distribution for each region. The central panel presents representative pressure–temperature (P–T) gradients for each subduction zone, with shaded regions indicating the estimated uncertainties of thermal regimes.

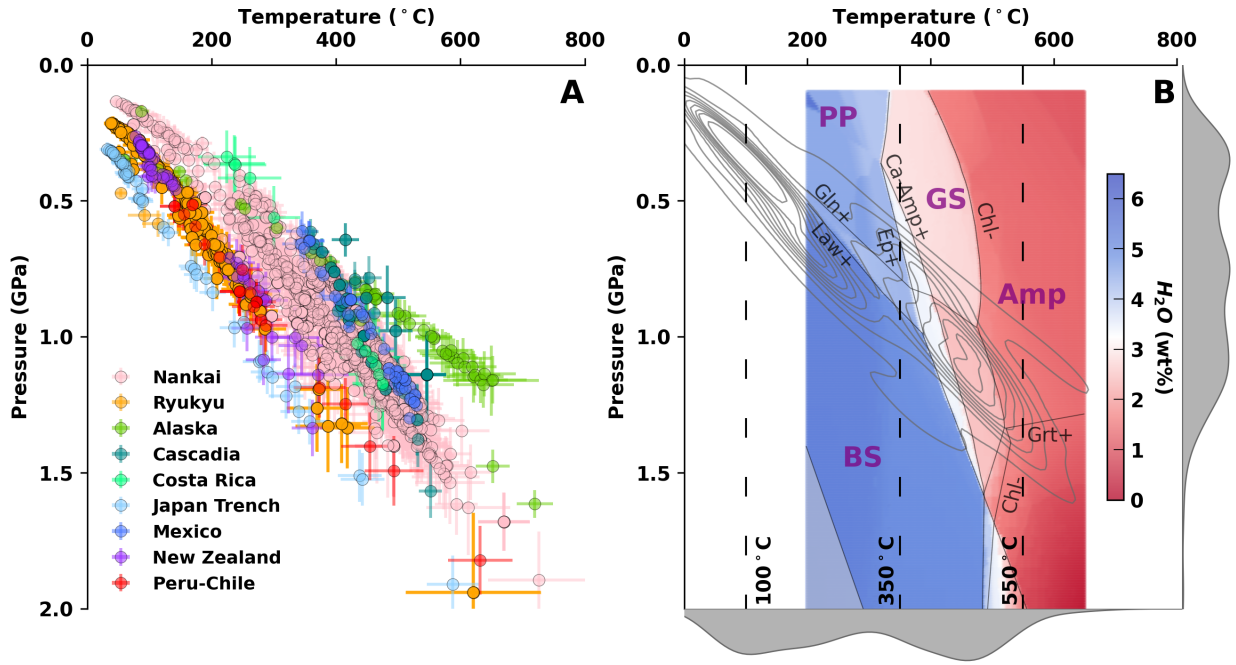


**Figure 2**: **SSEs align with metamorphic conditions of fluid release in subducting slabs.** (A) Pressure–temperature (P–T) conditions at the locus of slow slip events (SSEs) across nine subduction zones, color-coded by region. (B) Boundaries of major mineral dehydration reactions and consequent release of mineral-bound water (wt.%) from a representative metamorphic MORB (*41*) are illustrated in P-T space across the prehnite-pumpellyite (PP) blueschist (BS), greenschist (GS), and amphibolite (Amp) facies. Gray contours are the Kernel Density Estimate (KDE) of SSEs from (A), while gray marginal Probability Density Functions (PDF) of pressure and temperature are displayed on the right and bottom, respectively.

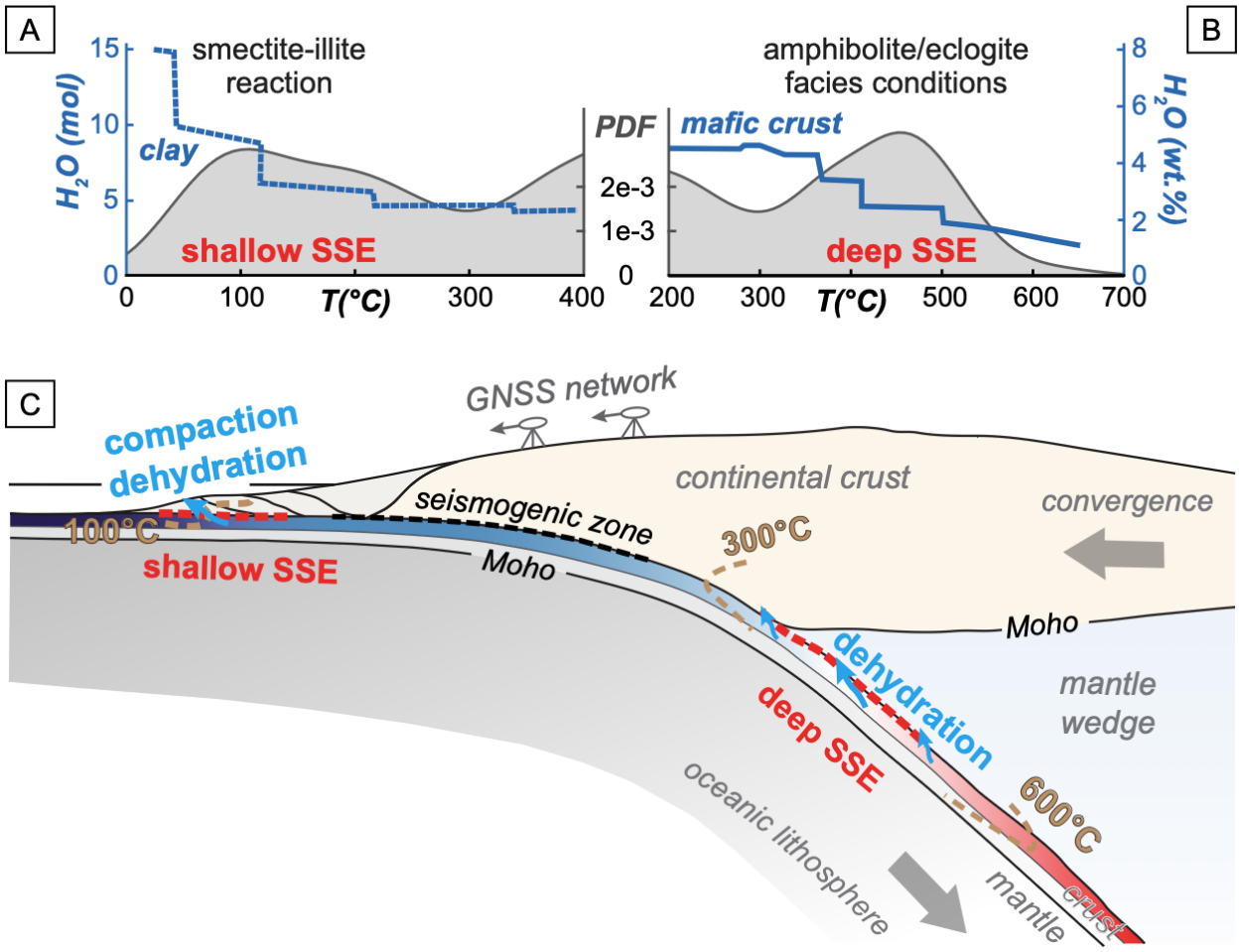


**Figure 3**: **Depth-dependent dehydration reactions define the thermal limits of slow slip activity.** Schematic cross-section of a subduction interface showing two distinct zones where slow slip events (SSEs) are observed. We differentiate shallow and deep SSEs based on the two main modes of the distribution of SSEs identified in Figure 2. Shallow SSEs (A) locate within the sedimentary cover at temperatures near 100$^o$C, coinciding with the smectite–illite transformation (*16, 43*). The panel shows the molar $H_2O$ release with increasing temperature for sedimentary rocks. Deep SSEs (B) lie deeper within the mafic oceanic crust, where greenschist to amphibolite/eclogite facies transitions occur between ~350$^o$C and 550$^o$C. Blue continuous line indicates the loss of water for a MORB undergoing prograde metamorphism along a P-T gradient of 13°C/km (from 200°C–0.4 GPa to 650°C–1.5 GPa; see Fig. 2).

# References and Notes


1. K. V. Steinbrugge, E. G. Zacher, D. Tocher, C. A. Whitten, C. N. Claire, Creep on the San Andreas fault. *Bulletin of the Seismological Society of America* **50** (3), 389–415 (1960), https://pubs.geoscienceworld.org/ssa/bssa/article-abstract/50/3/389/116001/Creep-on-the-San-Andreas-fault?redirectedFrom=fulltexthttps://pubs.geoscienceworld.org/ssa/bssa/article/50/3/389/116001/creep-on-the-san-andreas-fault.

2. H. F. Reid, *The Mechanism of the Earthquake. The California Earthquake of April 18, 1906: Rep. of the State Investigation Commiss. Vol. 2. P. 1*, Tech. rep., Carnegie Institution of Washington, Washington D. C. (1910).

3. J.-P. Avouac, From Geodetic Imaging of Seismic and Aseismic Fault Slip to Dynamic Modeling of the Seismic Cycle. *Annual Review of Earth and Planetary Sciences* **43** (1), 233–271 (2015), doi:10.1146/annurev-earth-060614-105302.

4. R. Bürgmann, The geophysics, geology and mechanics of slow fault slip. *Earth and Planetary Science Letters* **495**, 112–134 (2018), doi:10.1016/j.epsl.2018.04.062.

5. K. Obara, A. Kato, Connecting slow earthquakes to huge earthquakes. *Science (New York, N.Y.)* **353** (6296), 253–257 (2016), doi:10.1126/science.aaf1512.

6. A. Kato, Y. Ben-Zion, The generation of large earthquakes. *Nature Reviews Earth & Environment* **2** (1), 26–39 (2021), doi:10.1038/s43017-020-00108-w.

7. M. Arroyo-Solórzano, *et al.*, Impact of geodetic information, subduction zone segmentation, and slow-slip events in probabilistic seismic hazard: A case study for Costa Rica. *Geophysical Journal International* (2025), doi:10.1093/gji/ggaf204.

8. R. Jolivet, W. B. Frank, The Transient and Intermittent Nature of Slow Slip. *AGU Advances* **1** (1) (2020), doi:10.1029/2019AV000126.

9. S. Y. Schwartz, J. M. Rokosky, Slow slip events and seismic tremor at circum-Pacific subduction zones. *Reviews of Geophysics* **45** (3), n/a–n/a (2007), doi:10.1029/2006RG000208.

10. Y. Liu, J. R. Rice, Spontaneous and triggered aseismic deformation transients in a subduction fault model. *Journal of Geophysical Research: Solid Earth* **112** (B9) (2007), doi: 10.1029/2007JB004930, https://agupubs.onlinelibrary.wiley.com/doi/10.1029/2007JB004930.

11. X. Gao, K. Wang, Rheological separation of the megathrust seismogenic zone and episodic tremor and slip. *Nature* **543** (7645), 416–419 (2017), doi:10.1038/nature21389.

12. A. Beall, A. Fagereng, S. Ellis, Strength of Strained Two-Phase Mixtures: Application to Rapid Creep and Stress Amplification in Subduction Zone Mélange. *Geophysical Research Letters* **46** (1), 169–178 (2019), doi:10.1029/2018GL081252.

13. W. M. Behr, R. Bürgmann, What's down there? The structures, materials and environment of deep-seated slow slip and tremor. *Philosophical Transactions of the Royal Society A: Mathematical, Physical and Engineering Sciences* **379** (2193), 20200218 (2021), doi: 10.1098/rsta.2020.0218.

14. S. Michel, A. Gualandi, J.-P. Avouac, Interseismic Coupling and Slow Slip Events on the Cascadia Megathrust. *Pure and Applied Geophysics* **176** (9), 3867–3891 (2019), doi:10.1007/s00024-018-1991-x, http://link.springer.com/10.1007/s00024-018-1991-x.

15. C. H. Scholz, Earthquakes and friction laws. *Nature* **391** (6662), 37–42 (1998), doi:10.1038/34097.

16. D. M. Saffer, H. J. Tobin, Hydrogeology and Mechanics of Subduction Zone Forearcs: Fluid Flow and Pore Pressure. *Annual Review of Earth and Planetary Sciences* **39** (1), 157–186 (2011), doi:10.1146/annurev-earth-040610-133408.

17. J. Ampuero, A. M. Rubin, Earthquake nucleation on rate and state faults – Aging and slip laws. *Journal of Geophysical Research: Solid Earth* **113** (B1), 1–21 (2008), doi:10.1029/2007JB005082.

18. E. Bayart, I. Svetlizky, J. Fineberg, Slippery but Tough: The Rapid Fracture of Lubricated Frictional Interfaces. *Physical Review Letters* **116** (19), 194301 (2016), doi:10.1103/PhysRevLett.116.194301.

19. P. Segall, A. M. Rubin, A. M. Bradley, J. R. Rice, Dilatant strengthening as a mechanism for slow slip events. *Journal of Geophysical Research: Solid Earth* **115** (12), 1–37 (2010), doi:10.1029/2010JB007449.

20. A. J. Kotowski, W. M. Behr, Length scales and types of heterogeneities along the deep subduction interface: Insights from exhumed rocks on Syros Island, Greece. *Geosphere* **15** (4), 1038–1065 (2019), doi:10.1130/GES02037.1.

21. M. Soret, *et al.*, Deep crustal deformation driven by reaction-induced weakening. *Nature Communications* **16** (1), 6407 (2025), doi:10.1038/s41467-025-60692-7.

22. P. Romanet, H. S. Bhat, R. Jolivet, R. Madariaga, Fast and Slow Slip Events Emerge Due to Fault Geometrical Complexity. *Geophysical Research Letters* **45** (10), 4809–4819 (2018), doi:10.1029/2018GL077579.

23. C. Cattania, Complex Earthquake Sequences On Simple Faults. *Geophysical Research Letters* **46** (17-18), 10384–10393 (2019), doi:10.1029/2019GL083628.

24. Y. Ben-Zion, I. Zaliapin, Localization and coalescence of seismicity before large earthquakes. *Geophysical Journal International* **223** (1), 561–583 (2020), doi:10.1093/gji/ggaa315.

25. M. Wei, Y. Kaneko, Y. Liu, J. J. McGuire, Episodic fault creep events in California controlled by shallow frictional heterogeneity. *Nature Geoscience* **6** (7), 566–570 (2013), doi:10.1038/ngeo1835.

26. P. M. Barnes, *et al.*, Slow slip source characterized by lithological and geometric heterogeneity. *Science Advances* **6** (13), 1–10 (2020), doi:10.1126/sciadv.aay3314.

27. D. M. Saffer, L. M. Wallace, The frictional, hydrologic, metamorphic and thermal habitat of shallow slow earthquakes. *Nature Geoscience* **8** (8), 594–600 (2015), doi:10.1038/ngeo2490.

28. C. B. Condit, V. E. Guevara, J. R. Delph, M. E. French, Slab dehydration in warm subduction zones at depths of episodic slip and tremor. *Earth and Planetary Science Letters* **552**, 116601 (2020), doi:10.1016/j.epsl.2020.116601.

29. O. Oncken, S. Angiboust, G. Dresen, Slow slip in subduction zones: Reconciling deformation fabrics with instrumental observations and laboratory results. *Geosphere* **18** (1), 104–129 (2022), doi:10.1130/GES02382.1.

30. M. Kano, *et al.*, Development of a Slow Earthquake Database. *Seismological Research Letters* **89** (4), 1566–1575 (2018), doi:10.1785/0220180021.

31. K. Dascher-Cousineau, R. Bürgmann, Global subduction slow slip events and associated earthquakes. *Science Advances* **10** (35), 1–9 (2024), doi:10.1126/sciadv.ado2191.

32. G. P. Hayes, *et al.*, Slab2, a comprehensive subduction zone geometry model. *Science* **362** (6410), 58–61 (2018), doi:10.1126/science.aat4723.

33. P. England, On Shear Stresses, Temperatures, and the Maximum Magnitudes of Earthquakes at Convergent Plate Boundaries. *Journal of Geophysical Research: Solid Earth* **123** (8), 7165–7202 (2018), doi:10.1029/2018JB015907.

34. P. C. England, D. A. May, The Global Range of Temperatures on Convergent Plate Interfaces. *Geochemistry, Geophysics, Geosystems* **22** (8), 1–19 (2021), doi:10.1029/2021GC009849.

35. P. C. England, A. J. Smye, Metamorphism and Deformation on Subduction Interfaces: 1. Physical Framework. *Geochemistry, Geophysics, Geosystems* **24** (1) (2023), doi:10.1029/2022GC010644.

36. D. A. Oleskevich, R. D. Hyndman, K. Wang, The updip and downdip limits to great subduction earthquakes: Thermal and structural models of Cascadia, south Alaska, SW Japan, and Chile. *Journal of Geophysical Research: Solid Earth* **104** (B7), 14965–14991 (1999), doi:10.1029/1999JB900060.

37. P. E. van Keken, C. R. Wilson, An introductory review of the thermal structure of subduction zones: I—motivation and selected examples. *Progress in Earth and Planetary Science* **10** (1) (2023), doi:10.1186/s40645-023-00573-z.

38. J. A. D. Connolly, The geodynamic equation of state: What and how. *Geochemistry, Geophysics, Geosystems* **10** (10) (2009), doi:10.1029/2009GC002540.

39. T. J. B. Holland, R. Powell, An improved and extended internally consistent thermodynamic dataset for phases of petrological interest, involving a new equation of state for solids. *Journal of Metamorphic Geology* **29** (3), 333–383 (2011), doi:10.1111/j.1525-1314.2010.00923.x.

40. G. E. Bebout, P. Agard, K. Kobayashi, T. Moriguti, E. Nakamura, Devolatilization history and trace element mobility in deeply subducted sedimentary rocks: Evidence from Western Alps HP/UHP suites. *Chemical Geology* **342**, 1–20 (2013), doi:10.1016/j.chemgeo.2013.01.009.

41. A. Gale, C. A. Dalton, C. H. Langmuir, Y. Su, J. Schilling, The mean composition of ocean ridge basalts. *Geochemistry, Geophysics, Geosystems* **14** (3), 489–518 (2013), doi:10.1029/2012GC004334.

42. P. Vrolijk, On the mechanical role of smectite in subduction zones. *Geology* **18** (8), 703 (1990), doi:10.1130/0091-7613(1990)018⟨0703:OTMROS⟩2.3.CO;2.

43. O. Vidal, B. Dubacq, Thermodynamic modelling of clay dehydration, stability and compositional evolution with temperature, pressure and H2O activity. *Geochimica et Cosmochimica Acta* **73** (21), 6544–6564 (2009), doi:10.1016/j.gca.2009.07.035.

44. D. M. Saffer, D. A. Lockner, A. McKiernan, Effects of smectite to illite transformation on the frictional strength and sliding stability of intact marine mudstones. *Geophysical Research Letters* **39** (11), 2–7 (2012), doi:10.1029/2012GL051761.

45. S. Kodaira, *et al.*, High Pore Fluid Pressure May Cause Silent Slip in the Nankai Trough. *Science* **304** (5675), 1295–1298 (2004), doi:10.1126/science.1096535.

46. A. Fagereng, J. F. Diener, S. Ellis, F. Remitti, Fluid-related deformation processes at the up- and downdip limits of the subduction thrust seismogenic zone: What do the rocks tell us?, in *Geology and Tectonics of Subduction Zones: A Tribute to Gaku Kimura* (Geological Society of America), vol. 534, pp. 187–215 (2018), doi:10.1130/2018.2534(12).

47. H. Leah, *et al.*, Mixed Brittle and Viscous Strain Localization in Pelagic Sediments Seaward of the Hikurangi Margin, New Zealand. *Tectonics* **39** (8), 1–28 (2020), doi:10.1029/2019TC005965.

48. D. M. Veedu, S. Barbot, The Parkfield tremors reveal slow and fast ruptures on the same asperity. *Nature* **532** (7599), 361–365 (2016), doi:10.1038/nature17190.

49. P. Segall, J. R. Rice, Dilatancy, compaction, and slip instability of a fluid-infiltrated fault. *Journal of Geophysical Research: Solid Earth* **100** (B11), 22155–22171 (1995), doi:10.1029/95JB02403.

50. A. Fagereng, S. A. M. den Hartog, Subduction megathrust creep governed by pressure solution and frictional–viscous flow. *Nature Geoscience* **10** (1), 51–57 (2017), doi:10.1038/ngeo2857, http://www.nature.com/articles/ngeo2857.

51. L. L. Lavier, X. Tong, J. Biemiller, The Mechanics of Creep, Slow Slip Events, and Earthquakes in Mixed Brittle-Ductile Fault Zones. *Journal of Geophysical Research: Solid Earth* **126** (2), 1–27 (2021), doi:10.1029/2020JB020325.

52. A. Fagereng, G. W. B. Hillary, J. F. A. Diener, Brittle-viscous deformation, slow slip, and tremor. *Geophysical Research Letters* **41** (12), 4159–4167 (2014), doi:10.1002/2014GL060433.

53. Fagereng, A. Beall, Is complex fault zone behaviour a reflection of rheological heterogeneity? *Philosophical Transactions of the Royal Society A: Mathematical, Physical and Engineering Sciences* **379** (2193) (2021), doi:10.1098/rsta.2019.0421.

54. K. Heki, T. Kataoka, On the biannually repeating slow-slip events at the Ryukyu Trench, southwestern Japan. *Journal of Geophysical Research: Solid Earth* **113** (B11), 1–12 (2008), doi:10.1029/2008JB005739.

55. S. Sekine, H. Hirose, K. Obara, Along-strike variations in short-term slow slip events in the southwest Japan subduction zone. *Journal of Geophysical Research: Solid Earth* **115** (B9) (2010), doi:10.1029/2008JB006059.

56. S. Itaba, R. Ando, A slow slip event triggered by teleseismic surface waves. *Geophysical Research Letters* **38** (21), n/a–n/a (2011), doi:10.1029/2011GL049593.

57. T. Nishimura, T. Matsuzawa, K. Obara, Detection of short-term slow slip events along the Nankai Trough, southwest Japan, using GNSS data. *Journal of Geophysical Research: Solid Earth* **118** (6), 3112–3125 (2013), doi:10.1002/jgrb.50222.

58. T. Nishimura, Short-term slow slip events along the Ryukyu Trench, southwestern Japan, observed by continuous GNSS. *Progress in Earth and Planetary Science* **1** (1), 1–13 (2014), doi:10.1186/s40645-014-0022-5.

59. R. Takagi, K. Obara, T. Maeda, Slow slip event within a gap between tremor and locked zones in the Nankai subduction zone. *Geophysical Research Letters* **43** (3), 1066–1074 (2016), doi:10.1002/2015GL066987.

60. B. Rousset, *et al.*, A geodetic matched filter search for slow slip with application to the Mexico subduction zone. *Journal of Geophysical Research: Solid Earth* **122** (12), 498–10 (2017), doi:10.1002/2017JB014448, http://doi.wiley.com/10.1002/2017JB014448http://dx.doi.org/10.1002/2017JB014448.

61. Y. Tu, K. Heki, Decadal Modulation of Repeating Slow Slip Event Activity in the Southwestern Ryukyu Arc Possibly Driven by Rifting Episodes at the Okinawa Trough. *Geophysical Research Letters* **44** (18), 9308–9313 (2017), doi:10.1002/2017GL074455.

62. R. Takagi, N. Uchida, K. Obara, Along-Strike Variation and Migration of Long-Term Slow Slip Events in the Western Nankai Subduction Zone, Japan. *Journal of Geophysical Research: Solid Earth* **124** (4), 3853–3880 (2019), doi:10.1029/2018JB016738.

63. M. J. Ikari, *et al.*, Observations of Laboratory and Natural Slow Slip Events: Hikurangi Subduction Zone, New Zealand. *Geochemistry, Geophysics, Geosystems* **21** (2), 1–19 (2020), doi:10.1029/2019GC008717.

64. S. Xie, *et al.*, Slow Slip and Inter-transient Locking on the Nicoya Megathrust in the Late and Early Stages of an Earthquake Cycle. *Journal of Geophysical Research: Solid Earth* **125** (11), 1–22 (2020), doi:10.1029/2020JB020503, https://agupubs.onlinelibrary.wiley.com/doi/10.1029/2020JB020503.

65. T. Nishimura, Slow Slip Events in the Kanto and Tokai Regions of Central Japan Detected Using Global Navigation Satellite System Data During 1994–2020. *Geochemistry, Geophysics, Geosystems* **22** (2), 1–19 (2021), doi:10.1029/2020GC009329.

66. Y. Okada, T. Nishimura, T. Tabei, T. Matsushima, H. Hirose, Development of a detection method for short-term slow slip events using GNSS data and its application to the Nankai subduction zone. *Earth, Planets and Space* **74** (1), 18 (2022), doi:10.1186/s40623-022-01576-8.

67. Y. Okada, T. Nishimura, Systematic Detection of Short-Term Slow Slip Events in Southcentral Alaska. *Geophysical Research Letters* **50** (17), 1–9 (2023), doi:10.1029/2023GL104901.

68. S. Yabe, *et al.*, Eight-year catalog of deep short-term slow slip events at the Nankai trough based on objective detection algorithm using strain and tilt records. *Earth, Planets and Space* **75** (1), 13 (2023), doi:10.1186/s40623-023-01769-9.

69. M. Perry, C. Muller, M. Protti, L. Feng, E. M. Hill, Shallow Slow Slip Events Identified Offshore the Osa Peninsula in Southern Costa Rica From GNSS Time Series. *Geophysical Research Letters* **50** (20), 1–12 (2023), doi:10.1029/2023GL104771, `https://agupubs.onlinelibrary.wiley.com/doi/10.1029/2023GL104771`.

70. J. Jara, R. Jolivet, A. Socquet, D. Comte, E. Norabuena, Detection of slow slip events along the southern Peru - northern Chile subduction zone. *Seismica* **3** (1) (2024), doi:10.26443/seismica.v3i1.980, `https://seismica.library.mcgill.ca/article/view/980`.

71. L. Marill, D. Marsan, B. Rousset, A. Socquet, Geodetic Matched Filter Slow Slip Event Detection Along the Northern Japan Subduction Zones. *Journal of Geophysical Research: Solid Earth* **129** (9) (2024), doi:10.1029/2024JB029342.

72. A. Katsumata, *et al.*, Temporary slip speed increases during short-term slow slip events with durations of one to three hours. *Earth, Planets and Space* **76** (1), 45 (2024), doi:10.1186/s40623-024-01983-z.

73. G. Van Rossum, F. L. Drake, *Python 3 Reference Manual* (CreateSpace) (2009), `www.python.org`.

74. J. D. Hunter, Matplotlib: A 2D Graphics Environment. *Computing in Science & Engineering* **9** (3), 90–95 (2007), doi:10.1109/MCSE.2007.55.

75. D. Tian, *et al.*, PyGMT: A Python interface for the Generic Mapping Tools (2024), doi:10.5281/zenodo.11062720.

# Acknowledgments

The authors express their sincere gratitude to H.S. Bhat, O. Oncken, and G. Dresen for their valuable discussions regarding the manuscript.

**Funding:** J. J. acknowledges a MSCA Postdoctoral Fellowship (MSCA-101066069, project ERASMUS). R. J. acknowledges funding from the Institut Universitaire de France. This project received funding from the European Research Council (ERC) under the European Union's Horizon 2020 research and innovation program (Grant 758210 for project Geo4D and Grant 101125232 for project iQuake).

**Author contributions:** Conceptualization: J. J. and R. J. Data Curation: J. J., and M. S. Funding acquisition: J. J., R. J., and F. C. Formal analysis: J. J. Methodology: J. J., M. S., R. J., N. C., A. M., and F. C. Project administration: J. J. Resources: J. J., R. J., and F. C. Supervision: J. J., R. J., and F. C. Visualization: J. J., M. S., and R. J. Writing– original draft: J. J. Writing– review and editing: J. J., M. S., R. J., N. C., A. M., and F. C.

**Competing interests:** The authors declare no competing interests.

**Data and materials availability:** The SSE database used in this study is publicly available through the Slow Earthquake Database (*30*): `http://www-solid.eps.s.u-tokyo.ac.jp/~sloweq/`, which compiles events from multiple sources (*14, 31, 54–72*). All computations were carried out using Python 3.11 (*73*), and figures were produced using Matplotlib (*74*) and PyGMT (*75*).